Comparison of Methods for Far Zone Scattering from a Flat Plate and Cube *

R. J. Marhefka
T. J. Brinkley
The Ohio State University ElectroScience Laboratory
Department of Electrical Engineering
Columbus, Ohio 43212

Abstract

Different high frequency methods are used to analyze the backscatter and bistatic scattering from a flat plate and a cube. The results are compared and their validity is checked against method of moments and measurements. A newly developed far zone corner diffraction coefficient based on the latest equivalent current and PTD solutions cast in UTD form is discussed.

I Introduction

The validity of various methods for determining the far zone bistatic scattering from a flat plate and convex flat plate structure such as a cube is presented in this paper. This is accomplished by comparing the methods in various basic situations. The specific techniques to be compared in this study are the classical equivalent currents with "stripping" [1], the previous corner diffraction coefficient [1], the newly developed equivalent currents by Michaeli [2], and an extension to this method cast in the form of

*This work was supported in part by Contract No. F33615-86-K-1023 between Wright Patterson Air Force Base and The Ohio State University Research Foundation.

a Uniform Geometrical Theory of Diffraction (UTD) far zone corner diffraction coefficient [3]. In addition, the Method of Moments (MOM) using the Electromagnetic Surface Patch (ESP) code [4] and measurements from The Ohio State University ElectroScience Laboratories compact range are used to further validate the results.

A recent paper by Ludwig [5] compares three methods for backscattering from a cube, that is, the MOM using the Numerical Electromagnetics Code (NEC-MOM), physical optics (PO), and the previous UTD corner diffraction solution. In this paper, it will be shown that methods which give comparable results for backscatter can differ for bistatic scattering. The emphasis here is to present basic examples that can be used to validate existing codes and to suggest a numerically efficient and accurate method for convex flat plate structures to first order.

An approximate expression for the far zone field scattered by the vertex of a finite perfectly conducting wedge is presented in this regard. The solution is cast in the form of the UTD and is based on asymptotic equivalent currents found using modified Physical Theory of Diffraction (PTD) concepts [2,3]. The faces of the wedge must be flat (the normal to each individual face is a constant everywhere on the face except at the edge) and the edges must be straight. For plane wave incidence from an arbitrary direction, the first order contribution from each vertex to the far zone scattered field is obtained.

Since diffraction is a local phenomena at high frequencies the results obtained for a finite wedge may be applied to much more complex bodies made up of simple shapes. The field scattered by a three-dimensional shape constructed from flat plates may be approximated to first order as the sum of the contributions from each individual corner. The first order solution should be reasonably accurate in or near the specular regions as long as the object is convex. A convex body is defined here as a closed surface made up of flat plates such that all of the exterior wedge angles, taken between faces and exterior to the surface, are greater than 180 degrees. A simple example of an object that does not meet this requirement is a corner reflector. In this case, the effect of the interaction between the faces must be taken into account. Higher order effects such as double diffraction [6] and edge waves [7] are not considered here.

Note that the results presented in this paper are for a parallel ray type

solution, that is, for a radar cross section result. The NEC - Basic Scattering Code (NEC-BSC)[8] is a near zone formulated code, that is it has a finite range involved. The UTD solutions are slightly different for this non-parallel ray case. The capabilities of the NEC-BSC and a comparable far zone code called the RCS-BSC are discussed in Reference [9].

II Theoretical Background

There are many approximate solutions to the scattered field from a finite perfectly conducting wedge. Physical Optics and its extension the Physical Theory of Diffraction [10] is surface and edge current based. Geometrical Optics (GO) and its extensions the Geometrical Theory of Diffraction (GTD) [11] and the Uniform Geometrical Theory of Diffraction [12] are ray based. The Method of Equivalent Currents (MEC) [13] is an intermediate type solution that was developed to handle caustic regions in the GTD. This has been augmented with the concept of stripping to provide better answers for flat plate problems [1]. Recently, Michaeli [14] showed a more rigorous approach in deriving equivalent currents. This was shown to be related to the incremental length method of Mitzner [15] by Knott [16]. These equivalent currents still had singularity problems that have been remedied by Michaeli [2] using a skewed coordinate system. Ufimtsev also derived a similar solution [17,18].

The above solutions can be cast in a corner diffraction coefficient form. These UTD ray type solutions have the advantage of being efficient for far zone flat plate problems since only the fields scattered from the corners need to be added. It also has the advantage that the results correlate to the scattering centers seen in high resolution measurements. Just the corner diffraction coefficient forms are outlined in this section.

A previous diffraction coefficient for a corner formed by the intersection of two straight edges was derived by Burnside and Pathak [1]. It is based on the asymptotic evaluation of the radiation integral containing the equivalent currents of Ryan and Peters [13]. The result was then empirically modified so that the diffraction coefficient would not change sign abruptly as it passes through the false shadow boundaries. It was derived for spherical wave incidence and remains valid for cases when the diffraction point is near the

corner since the integral was evaluated for a saddle point near an end point; however, only the far zone result is shown here. The corner diffracted field due to one corner and one edge in the case of plane wave incidence and a far zone receiver is given by

$$
\begin{aligned}
\begin{bmatrix} E^c_{\beta_o} \\ E^c_{\phi} \end{bmatrix} &= -\begin{bmatrix} E^i_{\beta'_o}(Q_c)\, D^c_s(\phi,\phi',\beta_o,\beta_{oc}) \\ E^i_{\phi'}(Q_c)\, D^c_h(\phi,\phi',\beta_o,\beta_{oc}) \end{bmatrix} \frac{e^{-jks}}{s} \\
\begin{bmatrix} D^c_s \\ D^c_h \end{bmatrix} &= \mp\begin{bmatrix} C_s(Q_e) \\ C_h(Q_e) \end{bmatrix} \frac{\sqrt{\sin\beta_o \sin\beta_{oc}}}{(\cos\beta_{oc}+\cos\beta_o)} \frac{e^{-j\frac{\pi}{4}}}{\sqrt{2\pi k}} \qquad (1) \\
C_{s,h}(Q_e) &= \frac{-e^{-j\frac{\pi}{4}}}{2n\sqrt{2\pi k}\sin\beta_a}\{[D^c_o(\phi-\phi')+D^c_n(\phi-\phi')] \\
&\mp [D^c_o(\phi+\phi')+D^c_n(\phi+\phi')]\} \\
D^c_{o,n}(\psi) &= D_{o,n}(\psi)\left|F\left[\frac{\sin^2\beta_a a^{\mp}(\psi)}{2\pi a(\beta_{oc}+\beta_o)}\right]\right| \\
a(\beta) &= 2\cos^2\left(\frac{\beta}{2}\right), \quad a^{\mp}(\psi) = 2\cos^2\left(\frac{2n\pi N^{\mp}-\psi}{2}\right)
\end{aligned}
$$

where $N^{\mp}$ is the integer which most nearly satisfies $2n\pi N^{\mp} - \psi = \mp\pi$, and

$$
\begin{aligned}
D_{o,n}(\psi) &= \cot\left[\frac{\pi \mp \psi}{2n}\right] \\
\beta_a &= \frac{\pi + \beta_o - \beta oc}{2} \\
F(x) &= 2j\left|\sqrt{x}\right| e^{jx}\int_{|\sqrt{x}|}^{\infty} e^{-j\tau^2}\, d\tau
\end{aligned}
$$

where the angles are shown in Figure 1. The sign on the diffraction coefficient may be plus or minus depending on which endpoint of the edge is being considered. The correct sign in front of the $C_{s,h}$ terms in Equation 1 is chosen based on the direction edge vector shown in Figure 1.

It is assumed that the incident field, and therefore the scattered field, is a time harmonic field with time dependence given by $e^{j\omega t}$, which is suppressed.

The new far zone corner diffraction solution is based on the PTD and cast into the form of the MEC and then into a UTD diffraction coefficient. The details of this procedure are given in [3], while a brief outline of how this

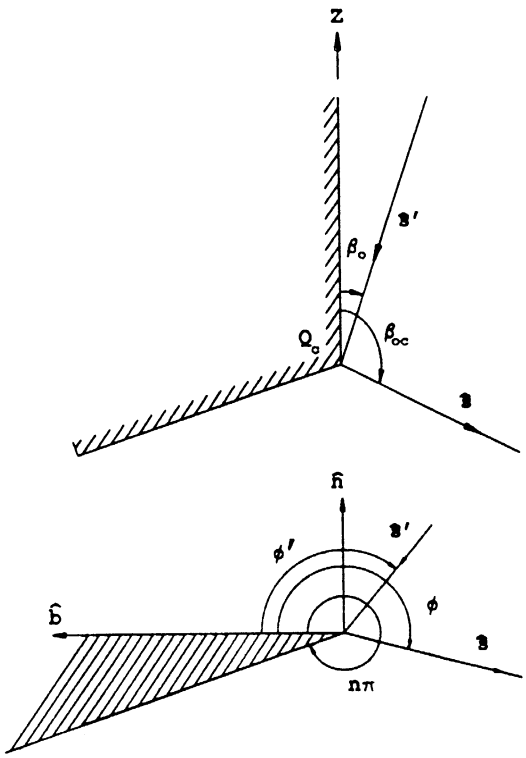

Figure 1: Definition of angles for the Previous Corner Diffraction Coefficients.

is done follows. The PO is first used to approximate the currents resulting in a double integral over the surface. Stokes theorem is then applied to reduce the equation to a line integral [19,20]. The Michaeli currents are added to produce a total first order MEC result. This integral is then evaluated using the method of stationary phase to obtain the contribution from each corner [21].

The new corner diffraction coefficients are given in a form similar to previous expressions for diffraction coefficients:

$$\begin{bmatrix} E^c_\beta \\ E^c_\phi \end{bmatrix} = \begin{bmatrix} D^c_s & D^c_2 \\ 0 & D^c_h \end{bmatrix} \begin{bmatrix} E^i_{\beta'} \\ E^i_{\phi'} \end{bmatrix} \frac{e^{-jks}}{s}$$

$$D^c_{s,h,2} = \pm \frac{j}{4\pi k} \left(\frac{1}{\cos\beta - \cos\beta'} \right) \left[d^{LPO}_{s,h,2} + d^{UTD}_{s,h,2} - d^{PO}_{s,h,2} \right]$$

where the plus or minus sign is chosen depending on which endpoint contribution is being calculated. The minus sign is used for the corner contribution associated with the negative t-axis, while the plus sign is used for the corner contribution associated with the positive t-axis. The edge

fixed coordinates shown in Figure 2 are chosen such that $\hat{n}$ is the outward normal of the O-face, $\hat{t}$ is tangent to the edge, the positive b-axis lies on the O-face, and $\hat{t} = \hat{b} \times \hat{n}$. The expressions for $d^{LPO}_{s,h,2}$, $d^{UTD}_{s,h,2}$, and $d^{PO}_{s,h,2}$ are given by (O-face contribution only)

$$
\begin{aligned}
d^{LPO}_{\substack{s \\ h,2}} &= \frac{1}{2} U^i c_{\substack{s \\ h,2}}(\gamma, \phi') \left\{ \left[\cot\left(\frac{\pi - (\gamma - \phi')}{4} \right) - \cot\left(\frac{\pi + (\gamma - \phi')}{4} \right) \right] \right. \\
&\mp \left. \left[\cot\left(\frac{\pi - (\gamma + \phi')}{4} \right) - \cot\left(\frac{\pi + (\gamma + \phi')}{4} \right) \right] \right\} \\
d^{UTD}_{\substack{s \\ h,2}} &= \frac{1}{n} c_{\substack{s \\ h,2}}(\alpha, \pi - \alpha) \left[\cot\left(\frac{\pi - (\alpha - \phi')}{2n} \right) \right. \\
&\mp \left. \cot\left(\frac{\pi - (\alpha + \phi')}{2n} \right) \right] \\
d^{PO}_{\substack{s \\ h,2}} &= \frac{1}{2} U^i c_{\substack{s \\ h,2}}(\alpha, \phi') \left\{ \left[\cot\left(\frac{\pi - (\alpha - \phi')}{4} \right) - \cot\left(\frac{\pi + (\alpha - \phi')}{4} \right) \right] \right. \\
&\mp \left. \left[\cot\left(\frac{\pi - (\alpha + \phi')}{4} \right) - \cot\left(\frac{\pi + (\alpha + \phi')}{4} \right) \right] \right\}
\end{aligned}
$$

where the + sign is associated with d^{LPO}_h, d^{LPO}_2, d^{UTD}_h, d^{UTD}_2, d^{PO}_h, and d^{PO}_2 while the $-$ sign is associated with the d^{LPO}_s, d^{UTD}_s, and d^{PO}_s terms. The functions c_s, c_h, and c_2 are given by

$$
\begin{aligned}
c_s(\delta, \epsilon) &= -\frac{\sin\beta}{\sin\beta'} \\
c_h(\delta, \epsilon) &= \frac{\sin\phi}{\sin\delta} \\
c_2(\delta, \epsilon) &= -\frac{\sin\beta}{\sin\delta} (\cot\beta \cos\phi + \cot\beta' \cos\epsilon) \\
U^i &= \begin{cases} 0 & , \pi - \phi' < 0 \\ 1 & , \pi - \phi' > 0 \end{cases} \\
\cos\gamma &= \frac{\sin\beta \cos\phi}{\sin\beta'} + \frac{(\cos\beta - \cos\beta')^2}{\sin\beta'(\sin\beta\cos\phi + \sin\beta'\cos\phi')} \\
\cos\alpha &= \frac{\sin\beta \cos\phi}{\sin\beta'} + \frac{(\cos\beta - \cos\beta')\cos\beta'}{\sin^2\beta'}
\end{aligned}
$$

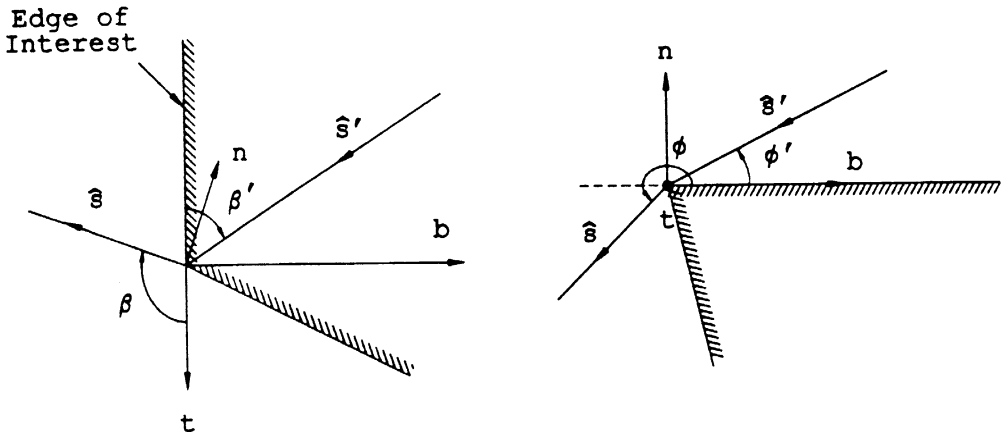

Figure 2: Definition of the Angles used in the New Corner Diffraction Coefficients.

from which γ and α are determined using

$$\cos^{-1}\mu = -j\ln\left(\mu+\sqrt{\mu^2-1}\right)$$

$$\sqrt{\mu^2-1} = \begin{cases} -\left|\sqrt{\mu^2-1}\right| & \mu<-1 \\ j\left|\sqrt{1-\mu^2}\right| & -1\le\mu\le 1 \\ \left|\sqrt{\mu^2-1}\right| & \mu>1 \end{cases}$$

Notice that γ and α do not correspond to physical angles and become complex for some cases. The angles β', ϕ', β, and ϕ are defined in Figure 2. Since only convex structures are considered here proper shadowing of the rays is fairly simple. The shadowing of the incident field is accounted for by $\vec{E}^i_{\beta'}$ and $\vec{E}^i_{\phi'}$ which are the components of the GO incident field. The shadowing of the diffracted ray is more complicated. The contributions from the LPO and PO components, $d^{LPO}_{h,s,2}$ and $d^{PO}_{h,s,2}$, are present everywhere. The UTD components, $d^{UTD}_{h,s,2}$, are shadowed like diffracted fields. They do not contribute if the observation point is inside the wedge ($\phi > n\pi$).

For the special case of a flat plate ($n = 2$) the contribution from both

faces may be found using

$$
\begin{aligned}
d^{LPO}_{\substack{s\\h,2}} &= \frac{1}{2}S^i c_{\substack{s\\h,2}}(\gamma,\phi')\left\{\left[\cot\left(\frac{\pi-(\gamma-\phi')}{4}\right)-\cot\left(\frac{\pi+(\gamma-\phi')}{4}\right)\right]\right.\\
&\mp \left.\left[\cot\left(\frac{\pi-(\gamma+\phi')}{4}\right)-\cot\left(\frac{\pi+(\gamma+\phi')}{4}\right)\right]\right\}\\
d^{UTD}_{\substack{s\\h,2}} &= \frac{1}{n}c_{\substack{s\\h,2}}(\alpha,\pi-\alpha)\left\{\left[\cot\left(\frac{\pi-(\alpha-\phi')}{4}\right)+\cot\left(\frac{\pi+(\alpha-\phi')}{4}\right)\right]\right.\\
&\mp \left.\left[\cot\left(\frac{\pi-(\alpha+\phi')}{4}\right)+\cot\left(\frac{\pi+(\alpha+\phi')}{4}\right)\right]\right\}\\
d^{PO}_{\substack{s\\h,2}} &= \frac{1}{2}S^i c_{\substack{s\\h,2}}(\alpha,\phi')\left\{\left[\cot\left(\frac{\pi-(\alpha-\phi')}{4}\right)-\cot\left(\frac{\pi+(\alpha-\phi')}{4}\right)\right]\right.\\
&\mp \left.\left[\cot\left(\frac{\pi-(\alpha+\phi')}{4}\right)-\cot\left(\frac{\pi+(\alpha+\phi')}{4}\right)\right]\right\}\\
S^i &= \begin{cases} -1 & ,\pi-\phi'<0\\ 1 & ,\pi-\phi'>0 \end{cases}
\end{aligned}
$$

where γ, α, and the other variables have been defined previously.

It is interesting to note that by writing the equations for the Michaeli equivalent currents and the new corner diffraction coeffients in cotangent form provide more insight into the connection of the new solutions with the previous methods. The new parameters separate out the optics currents and diffraction currents. This separation manifests itself in new parameters for the ϕ angles. They arise from the asymptotic evaluation of the currents in the skewed coordinate system chosen in physically meaningful directions. The LPO factor (γ) is related to the projection of the average of the incident and diffraction planes on to the plane of the plate [3]. The PO and UTD factor (α) relates to the projection of the Keller diffraction cone on to the plane of the plate. It is easy to see in this form that in the Keller directions the LPO and PO cancel, leaving the UTD result formally used in many solutions.

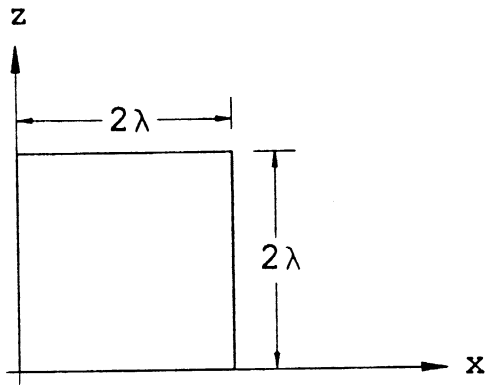

Figure 3: Two wavelength plate in the x-z plane.

III Comparisons

The first example compares the Ryan and Peters equivalent currents, the previous and new corner diffraction solutions. The simple example of backscatter from a two wavelength square plate lying in the x-z plane, as shown in Figure 3, is used. This illustrates that for backscatter these different methods produce very similar results, except for the very low level regions.

The co-polarized fields, in the principal plane, calculated using the three different methods are shown in Figures 4 and 5. All three methods give essentially the same results for the principal plane pattern cuts shown here. This is not surprising since the major contributions to the fields are the scattering from the two edges in their Keller cone directions. The new corner diffraction solution reduces to the Ryan and Peters equivalent current solution for points on the Keller cone [3], and the previous corner diffraction solution is essentially the same as Ryan and Peters equivalent current solution for most regions of space. The results in Figure 5 are for the horizontal ($\sigma_{\phi\phi}$) polarization. For a knife edged plate such as this, the scattered field should be zero in the plane of the plate. Note that this is not the case in

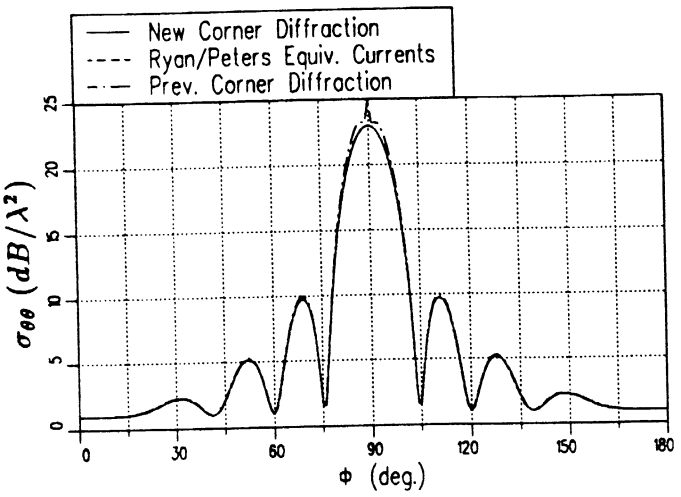

Figure 4: Backscatter from a 2 wavelength plate ($\theta = 90°$ pattern).

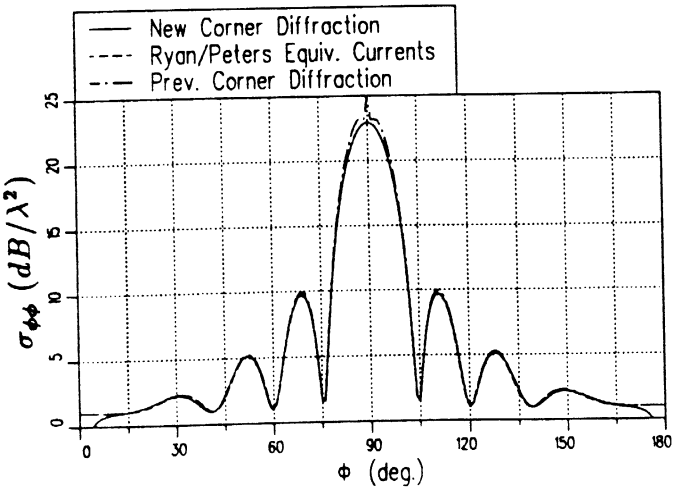

Figure 5: Backscatter from 2 wavelength plate ($\theta = 90°$ pattern).

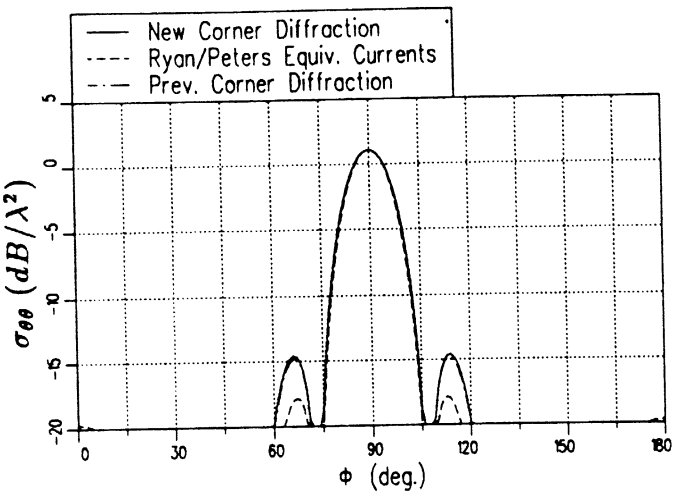

Figure 6: Backscatter from 2 wavelength plate ($\theta = 60°$ pattern).

these first order results. The higher order terms (i.e. the double, triple etc. diffractions) produce the null for this polarization when they are included.

For patterns away from the principal plane, the higher levels are the same but the lower levels differ. This is illustrated by taking a conical cut ($\theta = 60°$) for the two wavelength plate. The results for the same three methods used previously are shown in Figures 6 and 7. In this case the methods agree well for the main lobe, however, they differ in the lower levels of the pattern.

The differences in the three methods mentioned earlier are greatly increased for bistatic scattering problems. The bistatic scattering from a square plate two wavelengths on a side is examined to illustrate the point. The complete scattering matrix (all four values of σ) is found for a plate in the x-y plane with a fixed source located at $\theta^i = 45°$ and $\phi^i = 0°$ as shown in Figure 8. The results for the $\phi = 60°$ pattern cut are compared with the previous corner diffraction solution and Method of Moment calculations for co-polarized fields in Figures 9 and 10. Similarly the results for the cross-polarized fields are given in Figure 11 and Figure 12. Overall the new solution agrees well with the Method of Moment calculations and does not exhibit the discontinuities which appear near $\theta = 240°$ and $\theta = 300°$

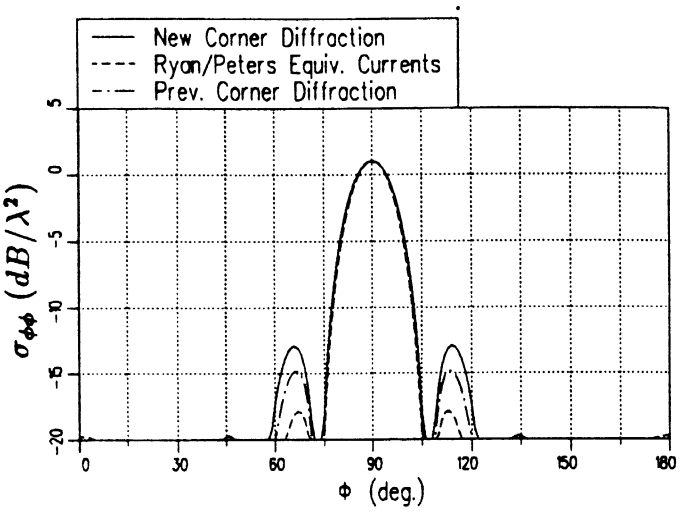

Figure 7: Backscatter from a 2 wavelength plate ($\theta = 60°$ pattern).

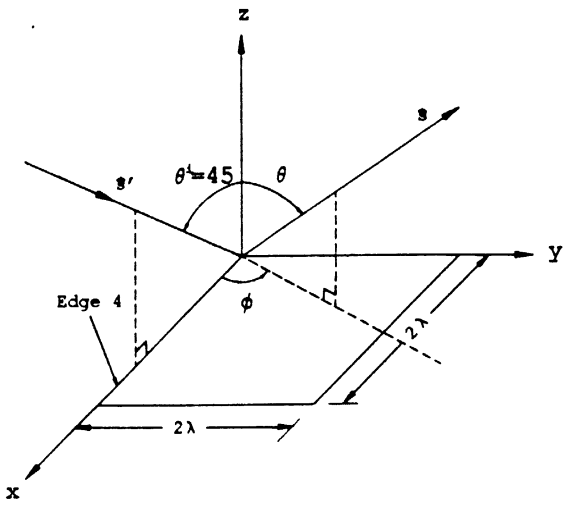

Figure 8: 2λ square plate in the x-y plane with a fixed source at $\theta^i = 45°$ and $\phi^i = 0$.

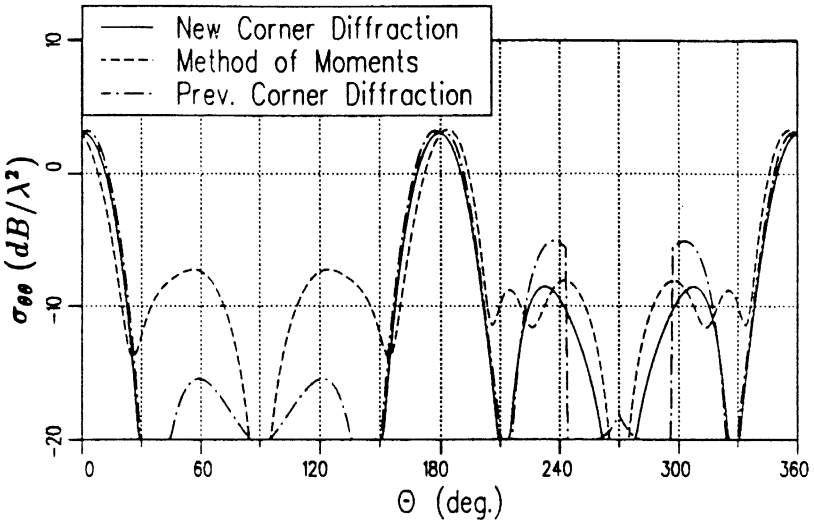

Figure 9: Co-polarized RCS in the $\phi = 60°$ plane of a 2λ square plate with a $\hat{\theta}^i$ polarized fixed source at $\theta^i = 45°$, $\phi^i = 0°$.

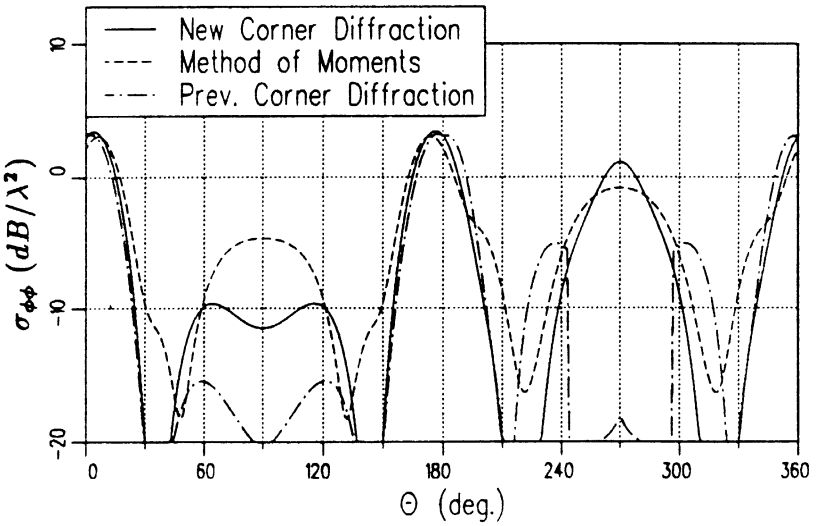

Figure 10: Co-polarized RCS in the $\phi = 60°$ plane of a 2λ square plate with a $\hat{\phi}^i$ polarized fixed source at $\theta^i = 45°$, $\phi^i = 0°$.

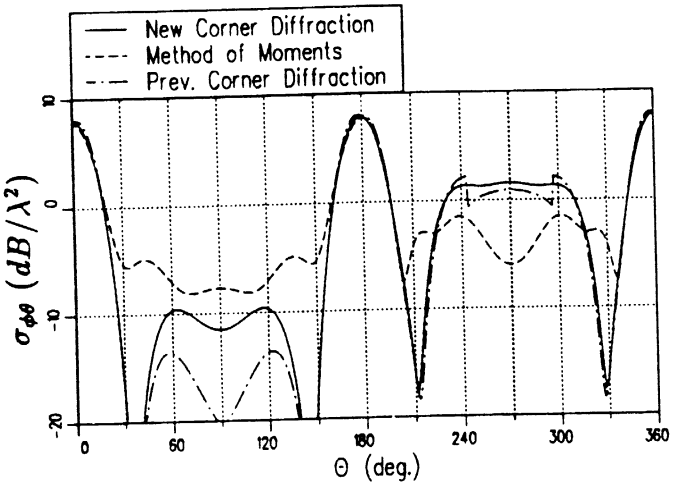

Figure 11: Cross-polarized RCS in the $\phi = 60°$ plane of a 2λ square plate with a $\hat{\theta}^i$ polarized fixed source at $\theta^i = 45°$, $\phi^i = 0°$.

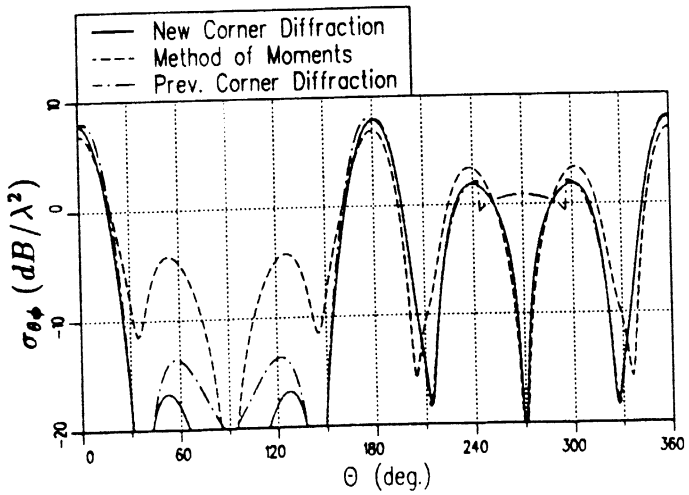

Figure 12: Cross-polarized RCS in the $\phi = 60°$ plane of a 2λ square plate with a $\hat{\phi}^i$ polarized fixed source at $\theta^i = 45°$, $\phi^i = 0°$.

in the previous corner diffraction solution. The discontinuities in the previous corner diffraction solution are caused by the so called false shadow boundaries where the associated two-dimensional problem passes through a shadow boundary, but the three-dimensional problem in reality does not. The Ryan and Peters equivalent current results are not shown here, but they behave differently for similar reasons; that is, the solution still contains two dimension information in regions that it should not. In the region from $\theta \approx 60°$ to 120° (i.e. near the plane of the plate) the new solution and the Method of Moments solution differ by more than 20 dB. It is suspected that most of these differences are due to the effects of higher order terms (double and triple diffraction, edge waves) which are not included in the new solution.

In this example the new solution is compared to backscatter measurements [22] made at 10 GHz on a 6" cube. The geometry of the cube, tilted 45° in the x-z plane, is illustrated in Figure 13. The results for the H-plane and E-plane patterns taken in the x-y plane are given in Figures 14 and 15, respectively. The results agree well to first order over most regions of the pattern. The discrepancies are probably due to a combination of higher order terms not being included in the analysis and in measurements errors. The error in the measurements is likely two fold. First the faces of the cube model were misaligned slightly so they did not form edges as sharp as may be required. Secondly, it seems that there was some deviation from the desired pattern cuts as can be seen from the lack of symmetry in the measured patterns. In any case, they confirm the validity of the new corner diffraction solution within first order accuracy for wedge type structures.

IV Discussion

The new corner diffraction coefficient in the above examples has been shown to provide improved results over other methods, especially in bistatic situations. The Michaeli equivalent currents have not been shown since they provide the same results as the new corner diffraction coefficient. Certain properties of these new solutions, however, may still cause patterns taken in some regions of space to be discontinuous.

It has been shown [2,3] that D_2^c and D_h^c do not tend to definite limits

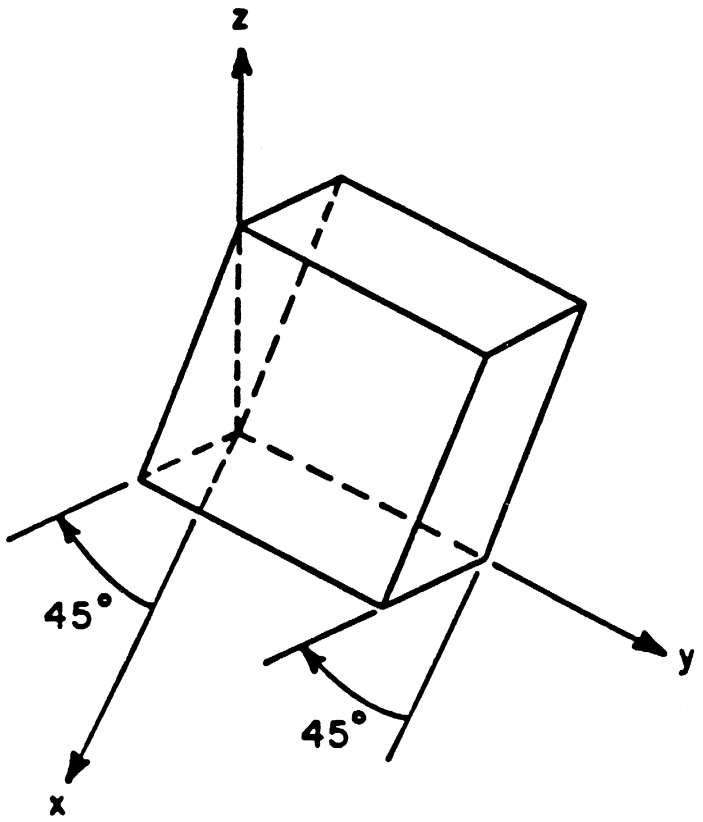

Figure 13: 6" Cube tilted 45° in the x-z plane.

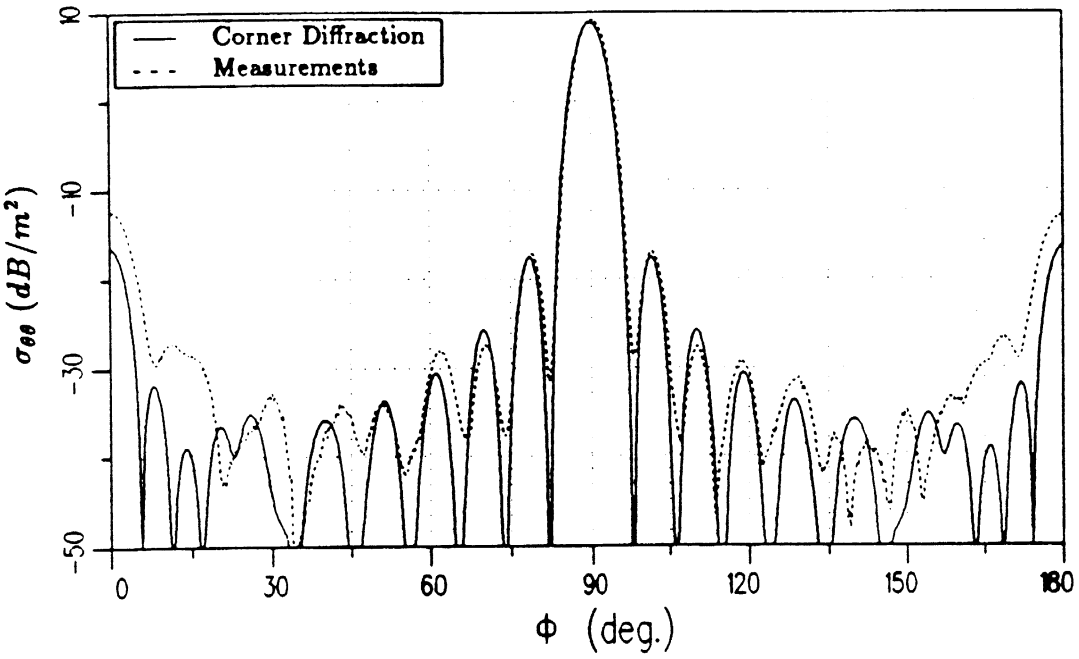

Figure 14: H-plane pattern for 6" cube tilted 45° in the x-z plane.

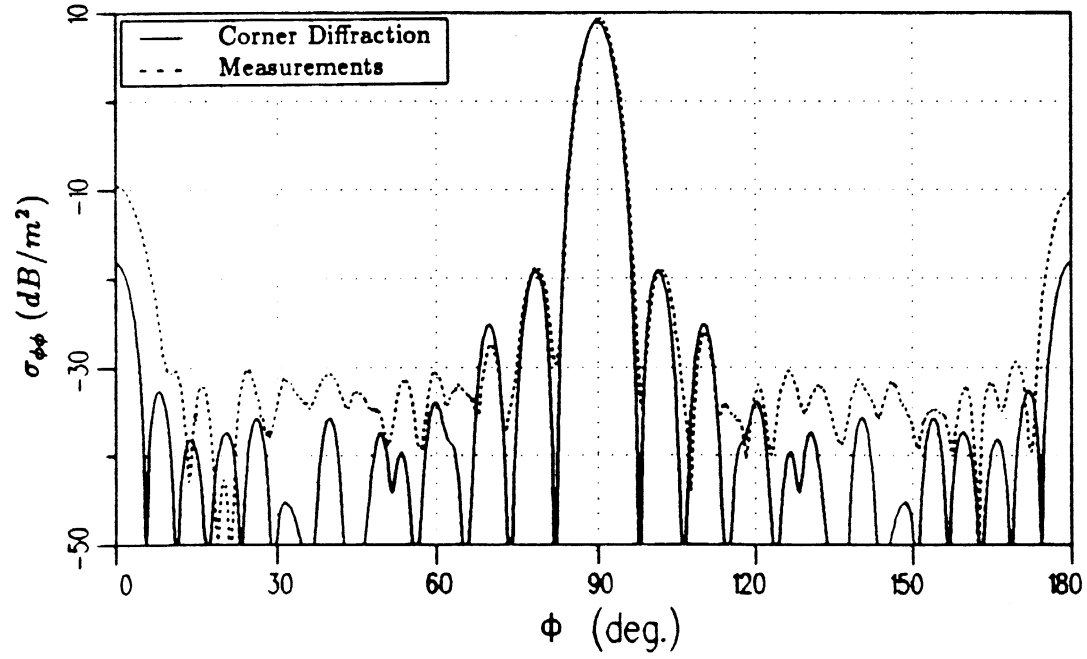

Figure 15: E-plane pattern for 6" cube tilted 45° in the x-z plane.

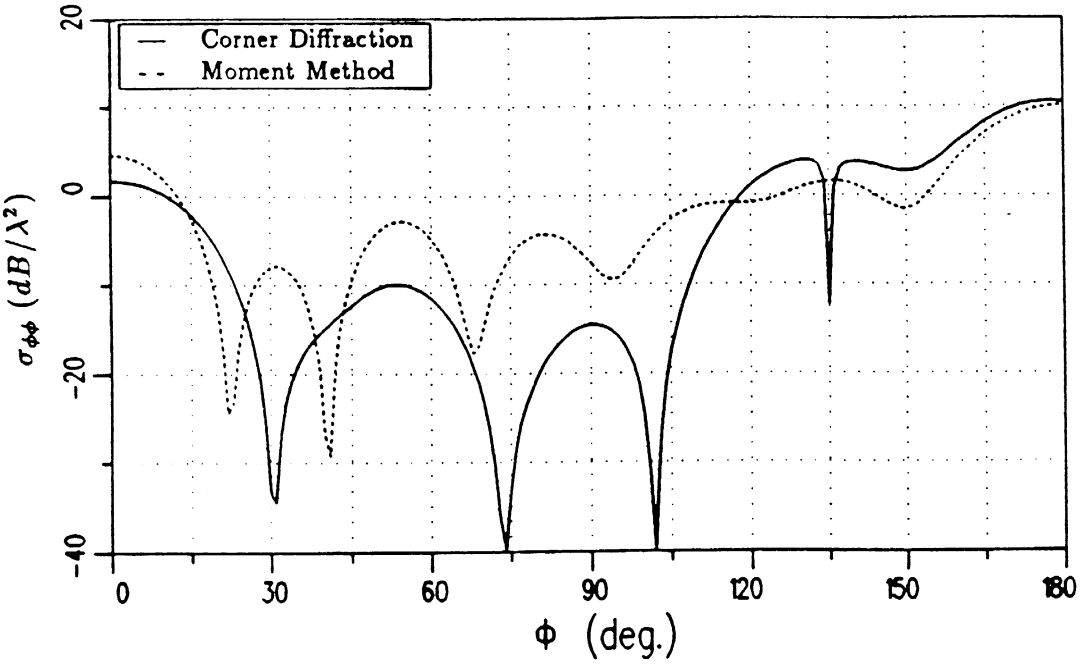

Figure 16: RCS for the $\theta = 89°$ cut of a 2λ square plate with a $\hat{\phi}^i$ polarized fixed source at $\theta^i = 45°$, $\phi^i = 0°$.

as $\hat{s} \rightarrow \hat{\sigma}$ (i.e. the intersection of the associated half-plane and the Keller cone), where $\hat{\sigma} = \hat{t}\sin\beta' + \hat{b}\cos\beta'$, but they remain bounded. In practice, this means that both D_2^c and D_h^c, and therefore E_β^c and E_ϕ^c, are discontinuous at this point in the pattern. A simple example illustrates how this discontinuity can affect a pattern. The bistatic RCS from the flat plate shown earlier in Figure 8 is considered. The source, linearly polarized in the $\hat{\phi}^i$ direction, remains fixed at $\theta^i = 45°$ and $\phi^i = 0°$ while the pattern is taken near the x-y plane ($\theta = 89°$). The bistatic RCS is given in Figures 16 and 17 for the co-polarized and cross polarized fields, respectively. The abrupt null at $\phi \approx 135°$ in the co-polarized pattern and the spike at the same location in the cross-polarized pattern are due to discontinuities in the contribution from edge 4 (indicated in Figure 8). The point $\phi \approx 135°$ coincides with $\beta_4 = \beta_4'$ and $\phi_4 \approx 0$ where β_4, β_4', and ϕ_4 are the edge fixed coordinates for edge 4. Due to the geometry $\hat{\beta}_4 \approx \hat{\phi}$ and $\hat{\phi}_4 \approx \hat{\theta}$ so the discontinuity in $\sigma_{\phi\phi}$ is due to the discontinuity in D_2^c and, likewise, the discontinuity in $\sigma_{\theta\phi}$ is due to the discontinuity in D_h^c.

Therefore, the discontinuity in the new diffraction coefficients at the

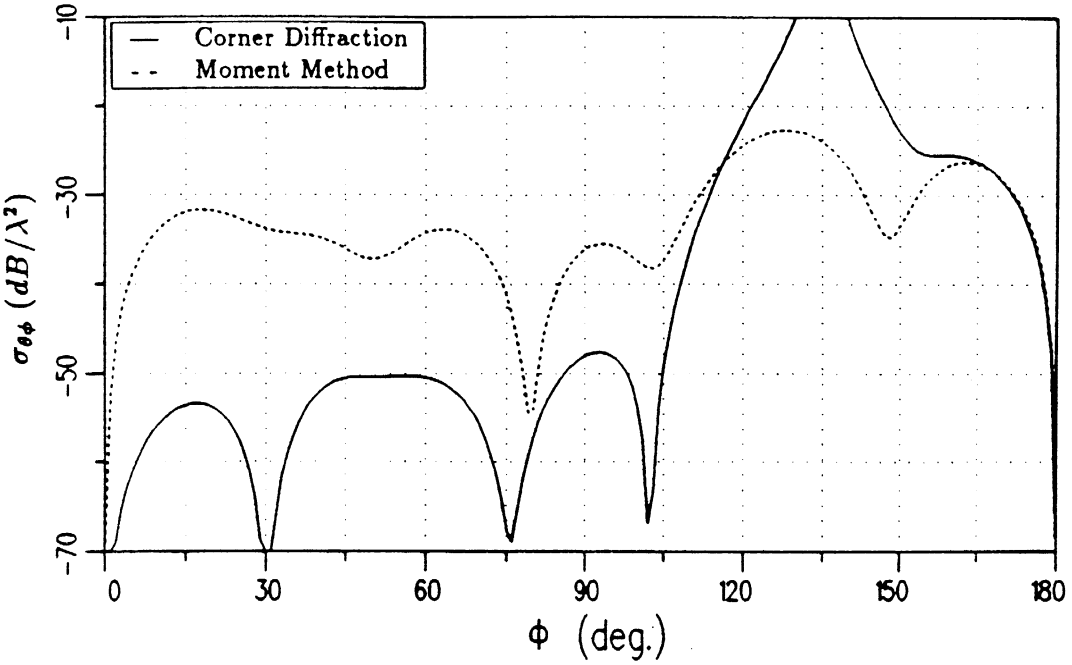

Figure 17: RCS for the $\theta = 89°$ cut of a 2λ square plate with a $\hat{\phi}^i$ polarized fixed source at $\theta^i = 45°$, $\phi^i = 0°$.

intersection of the Keller cone and the infinite half plane associated with the edge ($\beta = \beta'$ and $\phi = 0$) may be expected to cause discontinuities or narrow spikes depending on the polarization and the pattern cut. As the examples illustrate these disturbances only affect a typical pattern cut for around 5° to 10°. In addition, they are in the low level regions of the returns.

It is easily seen that the diffraction coefficients D_2^c and D_h^c are discontinuous as the source passes through the half plane $\phi' = \pi$. In the general case of bistatic scattering, these discontinuities in the sign of the field scattered by a corner will result in discontinuities in the total scattered field. However, the diffraction coefficients are continuous here ($\phi' = \pi$) for the special case of backscatter.

V Conclusions

The objective of this paper has been to compare different methods for the analysis of the high frequency far zone scattering from flat plate and convex flat plate type structures. Ryan and Peters equivalent currents and the previous corner diffraction coefficient are compared with the Michaeli equivalent currents and the new corner diffraction coefficient. The method of moments and measurements are also used to validate the solutions.

It has been shown that for backscatter all the methods compare reasonably within engineering accuracy. For bistatic scattering, however, the two dimensional nature of the old methods lead to inaccuracies. The newer methods, based on more rigorous three dimensional analysis, remove most of these problems.

A new corner diffraction coefficient is presented that provides an efficient and accurate solution to within first order. It provides the same level of accuracy as the Michaeli equivalent currents with the added benefit of not needing integrations for flat plates. All the optics and edge scattering effects have been lumped into the corners of the plate with nice physical interpretations.

References

[1] Sikta, F. A., W. D. Burnside, T. T. Chu, and L. Peters, Jr., "First-Order Equivalent Current and Corner Diffraction Scattering from Flat Plate Structures," *IEEE Trans. on Antennas and Propagation*, Vol. AP-31, No. 4, pp. 584–589, July 1983.

[2] Michaeli, A., "Elimination of Infinities In Equivalent Edge Currents, Part I: Fringe Current Components," *IEEE Trans. on Antennas and Propagation*, Vol. AP-34, No. 7, pp. 912–918, July 1986.

[3] Brinkley, T. J. and R. J. Marhefka, "Far Zone Bistatic Scattering from Flat Plates," Technical Report 718295-8, July 1988, The Ohio State University, ElectroScience Laboratory, Department of Electrical Engineering, prepared under Contract No. F33615-86-K-1023 for Wright Patterson Air Force Base.

[4] Newman, E. H. and R. L. Dilsavor, "A user's manual for the electromagnetic surface patch code: ESP version III," Report 716148, May 1987, The Ohio State University, ElectroScience Laboratory, prepared under Grant No. NSG 1613 with the National Aeronautics and Space Administration, Langley Research Center.

[5] Ludwig, A. C., "Backscattering from a Cube," Applied Computational Electromagnetic Society Journal and Newsletter, Vol. 2, No. 2, Fall 1987, pp. 55–73.

[6] Tiberio, R., M. Giuliano, G. Pelosi, and R. G. Kouyoumjian, "High-Frequency Electromagnetic Scattering of Plane Waves From Double Wedges," to be published.

[7] Sikta, F. A., "UTD Analysis of Electromagnetic Scattering by Flat Plate Structures," Ph.D. dissertation, The Ohio State University, Department of Electrical Engineering, Columbus, Ohio, 1981.

[8] R. J. Marhefka and W. D. Burnside, "Numerical Electromagnetic Code - Basic Scattering Code, NEC - BSC (Version 2), Part I: User's Manual," Technical Report 712242-14, December 1982, The Ohio State University ElectroScience Laboratory, Department of Electrical Engineering; prepared under Contract No. N00123-79-C-1469 for Naval Regional Contracting Office.

[9] Newman, E. H. and R. J. Marhefka, "An Overview of MM and UTD Methods at The Ohio State University," Proc. of the IEEE, to be published.

[10] Ufimtsev, P. Ya., "Method of Edge Waves in the Physical Theory of Diffraction," Air Force Systems Command, Foreign Tech. Div., Document ID No. FTD-HC-23-259-71, 1971 (Translation from the Russian "Method Krayevykh voin v fizicheskoy teorii difraktsi," Soviet Radio Publication House, Moscow, 1962).

[11] Keller, J. B., "Geometrical Theory of Diffraction," *J. Opt. Soc. of America*, Vol. 52, No. 2, pp. 116–130, Feb. 1962.

[12] Kouyoumjian, R. G., and P. H. Pathak, "A Uniform Geometrical Theory of Diffraction for an Edge in a Perfectly Conducting Surface," *Proc. IEEE*, Vol. 62, pp. 1448–1461, Nov. 1974.

[13] Ryan, C. E., Jr., and L. Peters, Jr., "Evaluation of Edge Diffracted Fields Including Equivalent Currents for the Caustic Regions," *IEEE Trans. on Antennas and Propagation*, Vol. AP-17, pp. 292–299, May 1969.

[14] Michaeli, A., "Equivalent Edge Currents for Arbitrary Aspects of Observation," *IEEE Trans. on Antennas and Propagation*, Vol. AP-32, No. 3, pp. 252–258, March 1984.

[15] Mitzner, K. M., "Incremental Length Diffraction Coefficients," Northrop Corp., Aircraft Division, Tech. Rep. No. AFAL-TR-73-296, April 1974.

[16] Knott, E. F., "The Relationship Between Mitzner's ILDC and Michaeli's Equivalent Currents," *IEEE Trans. on Antennas and Propagation*, Vol. AP-33, No. 1, pp. 112–114, January 1985.

[17] Ufimtsev, P. Ya., and D. I. Butorin, "Explicit Expressions for an Acoustic Edge Wave Scattered by an Infinitesimal Edge Element," *Sov. Phys. Acous.*, Vol. 34, No. 4, pp. 283–287, July–August 1986.

[18] Ufimtsev, P. Ya., "A New Mathematical Formulation of the Physical Theory of Diffraction," submitted to *IEEE Proc.* for publication.

[19] Buyukdura, O. M., R. J. Marhefka, and W. Ebihara, "Radar Cross Section Studies, Phase III," Technical Report 716622-1, The Ohio State University, ElectroScience Laboratory, April 1986.

[20] Gordon, Willliam B., "Far-Field Approximations to the Kirchoff-Helmholtz Representations of Scattered Fields," *IEEE Trans. on Antennas and Propagation*, pp. 590–592, July 1975.

[21] Buyukdura, O. M., personal communication.

[22] Dominek, A.K., personal communication.